Applied Surface Science 530 (2020) 147301

Contents lists available at ScienceDirect

Applied Surface Science

journal homepage: www.elsevier.com/locate/apsusc

Enhancement of the quantum capacitances of group-14 elemental two-dimensional materials by Ti-doping: A first principles study

Juven Rihm[a], Eun Seob Sim[a], Sung Beom Cho[b,*], Yong-Chae Chung[a,*]

[a] Division of Materials Science and Engineering, Hanyang University, Seoul 04763, Republic of Korea
[b] Virtual Engineering Center, Korea Institute of Ceramic Engineering and Technology, Jinju, Republic of Korea

ARTICLE INFO

Keywords:
Electric double layer capacitor
First-principle calculations
2D materials
Quantum capacitance
Doping

ABSTRACT

Group-14 elemental two-dimensional materials are a key material for future supercapacitors because of their various advantages compared to activated carbon. However, the lack of density of states (DOS) near the Fermi level (E_F) of these materials is one of the limiting factors for the performance of supercapacitors, especially for electric double-layer capacitors (EDLCs). In this study, Ti-doping was investigated as a strategy for providing a large amount of DOS near the E_F. By using density functional theory calculations, it was confirmed that the d band of the Ti atom provides additional DOS to the materials. The calculated quantum capacitances and the surface charge densities of the doped systems were enhanced overall in both their gravimetric and specific aspects thanks to the increased DOS near the E_F. In addition, it was revealed that Ti-doped silicene has superior characteristics at the low voltage range compared to other materials. These findings may provide practical guidelines for improving the performance of EDLCs.

1. Introduction

With increasing concern over the global energy supply, the importance of environmentally friendly and sustainable energy storage systems (ESS) is increasing. Recently, electric double-layer capacitors (EDLCs) have been investigated due to balanced energy-power density compared to conventional batteries and capacitors [1]. In EDLCs, the electric energy is electrochemically stored by the reversible adsorption reaction of ions in electrolyte onto electrode materials. The charge separation by the adsorption of ions leads to the creation of capacitance, and the discharging mechanism is only the desorption of ions. Such a simple charging mechanism leads to a long cycle life, wide operation temperature range, fast charge/discharge rate, and no memory effect. These features make EDLCs more versatile for energy conversion applications where a short charging/discharging process is repeated. At present, EDLCs are exploited for ESS by playing a complementary role with conventional batteries.

For high-performance EDLCs, electrode materials should be designed to maximize the charge storage from reversible ion adsorption. Recently, two-dimensional (2D) materials are being widely studied for EDLCs [2,3] because of their various advantages compared to activated carbon [4–9], which is a conventional electrode material. The 2D materials can provide an extremely large surface area for ion adsorption and a wider materials choice range. In particular, group-14 elemental two-dimensional materials (ETDMs) such as graphene, silicene, and germanene have shown great potential as EDLCs due to their conductivity and amount of adsorption sites [10–13]. However, the lack of density of states (DOS) near the Fermi level (E_F) of these materials is one of the limiting factors for the performance of EDLC. DOS is one of the critical criteria for determining the charge storage capacity because it provides room for transferred electrons in ion adsorption. This contribution can be verified by the quantum capacitance (C_Q), and it becomes a more serious limiting factor under low applied potential. Therefore, a strategy for enhancing DOS near the E_F of ETDMs should be established for enhancing the performance of EDLC.

In this study, we carried out density functional theory (DFT) calculations to investigate the Ti-doping strategies of various ETDMs for enhancing the C_Q. By comparing the electronic structures of pristine ETDM systems and Ti-doped systems, the effects of Ti-doping on the band structure, DOS, and C_Q were confirmed. We determined that Ti doping deforms the π-bonds network, which forms the Dirac cone near the E_F of ETDMs. On the other hand, the prosperous state of Ti 3d orbitals introduces a flat band near the E_F of the ETDMs. The large and sharp shape of the DOS plot leads to high C_Q near the low applied voltage. Furthermore, it also affects the gravimetric and specific performances, which are important criteria for a practical design for EDLCs. This shows that it is practical for the doping approach to have wide tunability for electronic structure and C_Q.

* Corresponding authors.
E-mail addresses: csb@kicet.re.kr (S.B. Cho), yongchae@hanyang.ac.kr (Y.-C. Chung).

https://doi.org/10.1016/j.apsusc.2020.147301
Received 26 April 2020; Received in revised form 6 July 2020; Accepted 16 July 2020
Available online 21 July 2020
0169-4332/

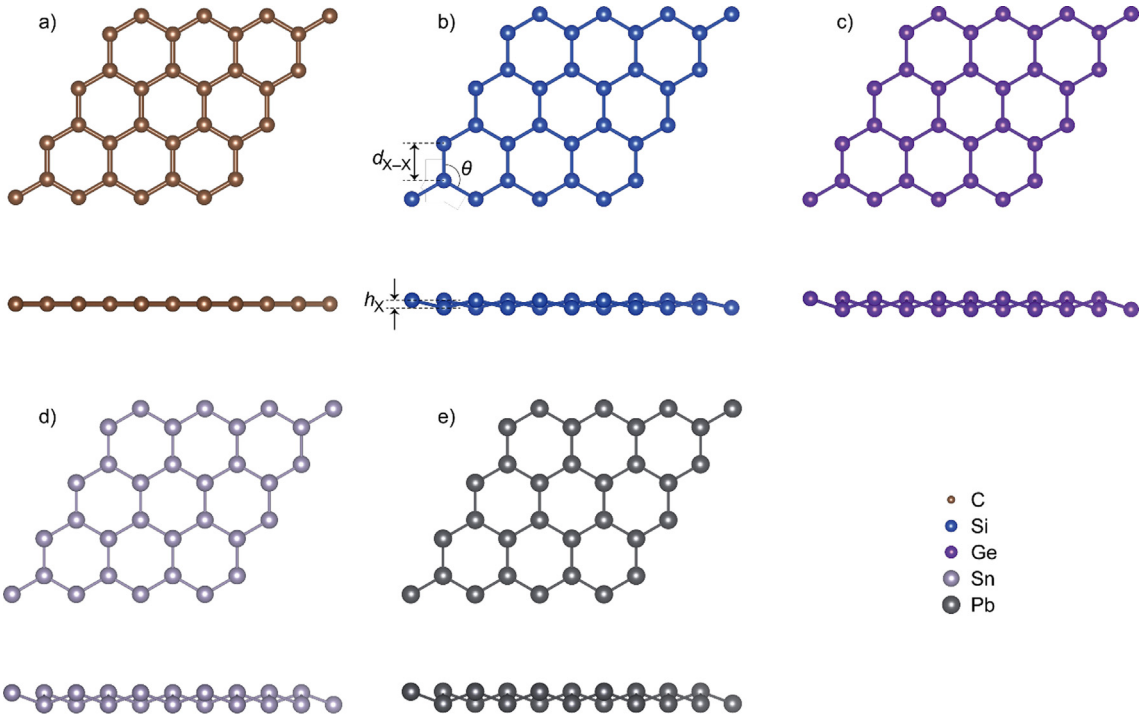

Fig. 1. Geometric structures of pristine systems with a top view (top panel) and front view (bottom panel). The bond length between two X atoms d_{X-X}, the buckling height h_X, and the bond angle θ is indicated on the structure of pristine silicene, where X represents an atom in group-14 elements.

2. Calculation methods

DFT calculations were conducted using the Vienna Ab-initio Simulation Package (VASP) [14–17]. The ion cores were described with projector augmented wave (PAW) pseudopotential methods [18,19], and generalized gradient approximation (GGA) [20,21] in the form of the Perdew–Burke–Ernzerhof (PBE) functional [22] was adopted to express the exchange–correlation energy functional. The kinetic cutoff energy was taken to be 500 eV with the plane-wave basis set. The pristine and Ti-doped ETDMs of the group-14 elements were modeled as 4 × 4 supercell structures. The supercell structures of the pristine systems consist of 32 atoms of a single element in group 14, as shown in Fig. 1. For each of the systems, one atom was substituted with a Ti atom to model the Ti-doped system. The spin–orbit coupling (SOC) effect was considered in pristine and Ti-doped systems where Pb atoms were used [23]. A 12 × 12 × 1 k-point mesh generated by the Γ-centered Monkhorst–Pack scheme [24] was used for the Brillouin zone integration, and a Gaussian smearing method with a width of 0.1 eV was used to describe the partial occupancies of the electrons. All the self-consistent loops were iterated until the total energy difference of the systems between the adjacent iterating steps became less than 10^{-5} eV/cell. Geometric optimization was carried out until the Hellmann–Feynman force on each atom was less than 0.02 eV/Å. To avoid direct interaction between the adjacent periodic images, the pristine and Ti-doped systems were modeled with a vacuum spacing of 15 Å. Strict energy convergence tests were performed for pristine and Ti-doped systems.

The quantum capacitance is defined as $C_Q = \mathrm{d}\sigma/\mathrm{d}\phi$, where σ is the excess charge density, and ϕ is the applied voltage. The excess charge density will also be called the surface charge density because the materials are two-dimensional. The value of σ can be calculated using the following formula [25]:

$$\sigma = e\int_{-\infty}^{\infty} D(E)[f(E) - f(E + e\phi)]\mathrm{d}E \quad (1)$$

where $e \approx 1.602 \times 10^{-19}$ C is the elementary charge, $D(E)$ is the density of states of the supercell system, $f(E)$ is the Fermi–Dirac distribution function, and E is the energy relative to E_F. Substituting this into the definition of C_Q yields the following formula:

$$C_Q = \frac{e^2}{4kT}\int_{-\infty}^{\infty} D(E)\mathrm{sech}^2\left(\frac{E + e\phi}{2kT}\right)\mathrm{d}E \quad (2)$$

where $k \approx 8.617$ eV/K is the Boltzmann constant, and T is the room temperature, which is defined as 300 K in this study.

3. Results and discussion

3.1. Geometric and electronic properties of pristine systems

The geometric structures of pristine ETDM systems were first investigated. All the ETDMs have honeycomb-like structures, and their lattice parameters and buckling heights are summarized in Table 1, which is consistent with the previous results [26–38]. Among them, graphene has the smallest lattice parameter. This is not only due to the smallest atomic number, but also due to the absence of buckling. All the bonding between the carbon atoms consists of sp^2 hybridized orbitals and delocalized π bonds with other carbon atoms via the p_z orbitals. However, other ETDMs except for graphene all have mixed sp^2–sp^3 hybridizations leading to structural buckling [39–43]. The buckling heights of ETDMs depend on the contribution of sp^3. Thus, stronger sp^3 hybridization leads to a larger buckled structure.

To understand the effect of a mixed sp^2–sp^3 contribution, we

Table 1
Geometric parameters of pristine systems. X represents an atom in the group-14 elements (C, Si, Ge, Sn, or Pb) of each system. The lattice parameter is a, the bond length between two X atoms is d_{X-X}, the buckling height is h_X, and the bond angle is θ, as indicated in Fig. 1.

	a (Å)	d_{X-X} (Å)	h_X (Å)	θ (°)
Graphene	2.47	1.43	0.000	120.0
Silicene	3.87	2.28	0.454	116.1
Germanene	4.06	2.44	0.690	112.4
Stanene	4.67	2.83	0.856	111.3
Plumbene	4.93	2.99	0.923	110.9

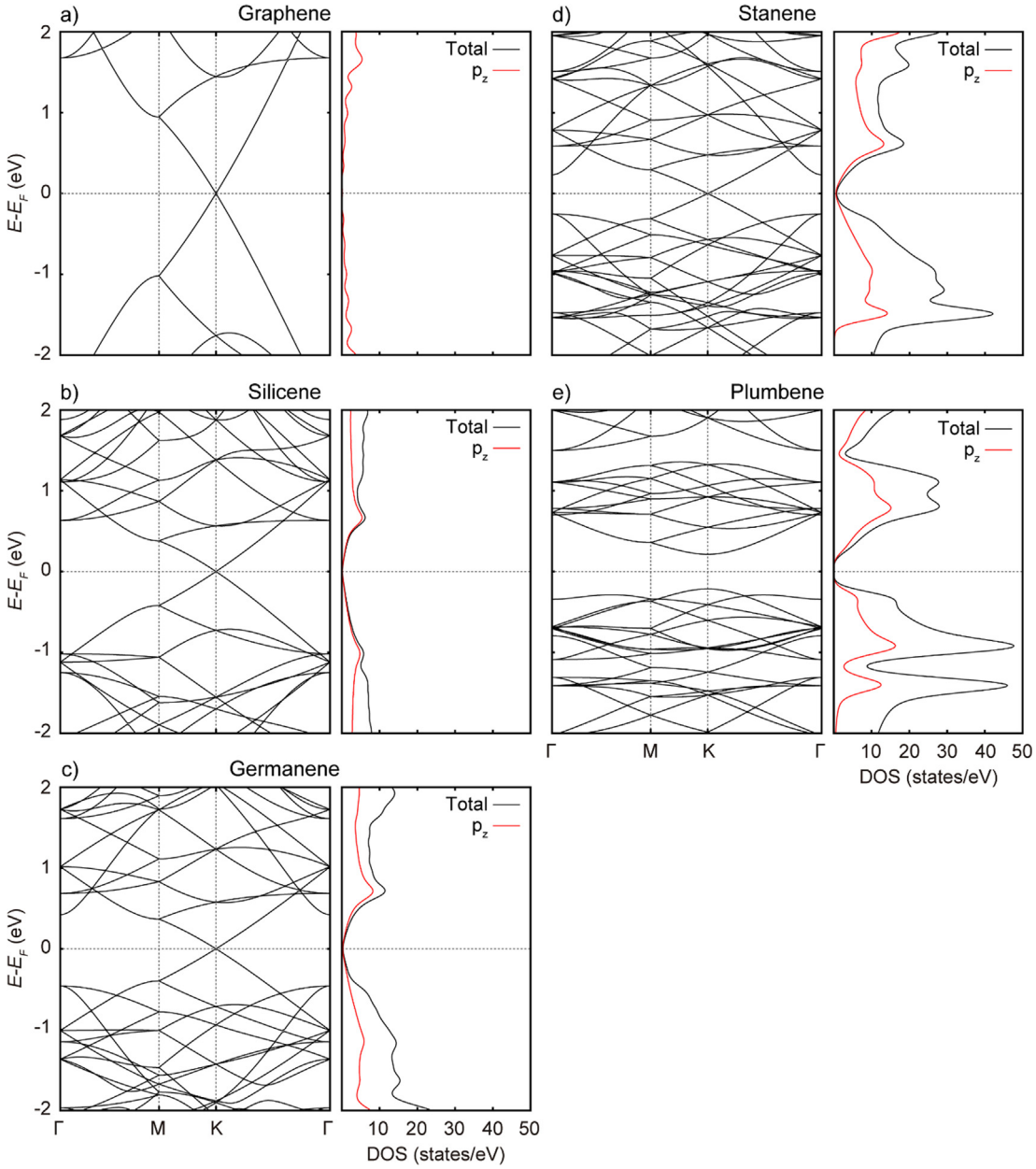

Fig. 2. Electronic band structures and projected density of states (PDOS) of pristine systems. The horizontal dashed lines represent the Fermi level (E_F).

investigated the electronic band structure and DOS, as shown in Fig. 2. From the band structure of all ETDMs except for plumbene, the Dirac cones are clearly visible at *K* point from graphene to stanene. The Dirac cone is the linear band crossing of the π and π* bands [32], and these bands are derived from the p_z orbitals. Graphene, which has no contribution of sp^3, has its DOS near the E_F, which is identical to the p_z states. On the other hand, the proportion of the p_z orbitals to the total DOS becomes smaller as the atomic number increases. This is because the contribution of sp^3 to mixed sp^2–sp^3 hybridization becomes more dominant from silicene to plumbene. Despite the smaller contribution of the p_z orbitals, the Dirac cone is still observable in all the ETDMs except for plumbene. It is beneficial for electronic mobility, but its low DOS near the E_F is not suitable for high quantum capacitance. In the case of plumbene, the SOC effects are strong enough to split the bands which eventually destroys the Dirac cone and opens the band gap. The opened gap leads to absence of DOS near the E_F which is detrimental to quantum capacitance.

3.2. Quantum capacitances and surface charges of pristine systems

The quantum capacitances (C_Q) and the surface charge densities (σ) of pristine systems are calculated and are shown in Fig. 3a and b, respectively. The lack of DOS near the E_F leads to a similar valley-like C_Q at the low voltage range. In particular, it is clearly shown that the C_Q of graphene is much lower than that of other systems in the applied voltage range. The σ of pristine graphene is very small in all ranges of the voltage. This pattern implies that pure graphene without any modification is not an appropriate material to be used for EDLCs because of the low accumulation of charges onto the material with respect to the applied bias. It is also shown that the C_Q of plumbene at no bias is approximately 0 μF/cm^2. This is due to the absence of DOS near the E_F caused by the SOC of plumbene. On the other hand, the larger DOS of the deeper conduction state ($E - E_F \approx 0.6$ eV), which came from the sp^2–sp^3 hybridization, induced the local maximum around an applied bias of −0.7 V for the other ETDMs. In addition, the sharp increase of DOS of stanene and plumbene at the valence state induced the sharp

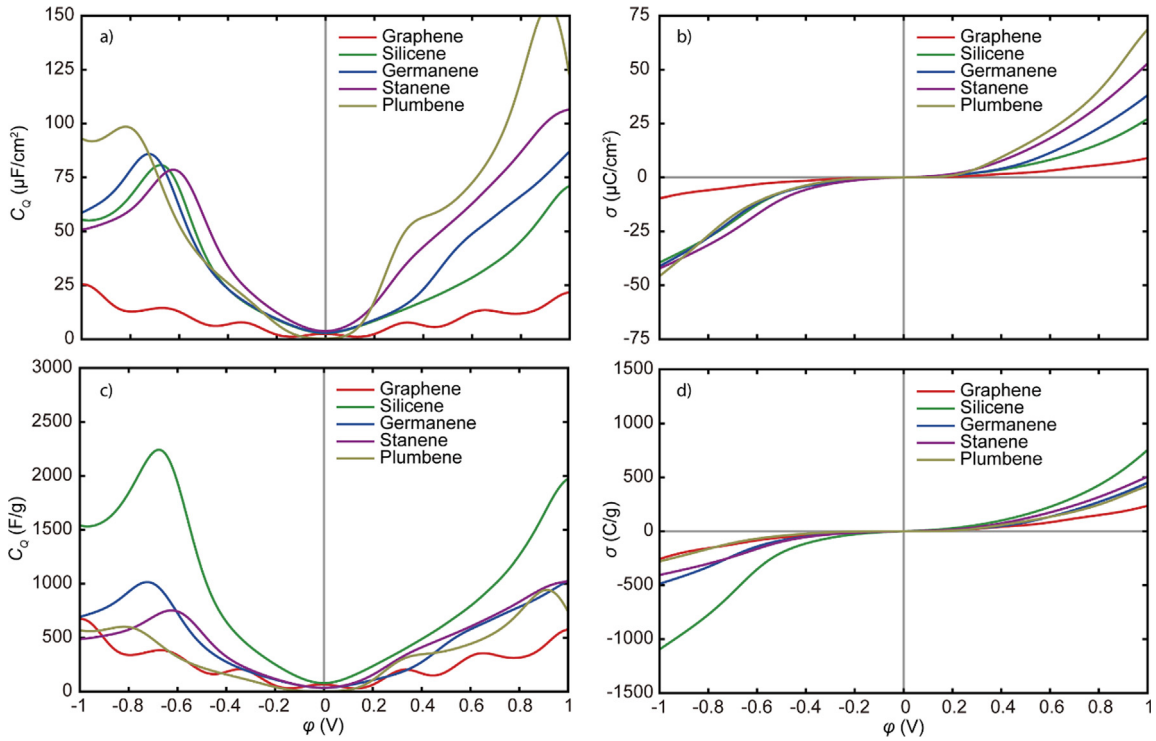

Fig. 3. (a) The quantum capacitances (C_Q) and (b) the excess charge densities (σ) of pristine systems with a specific unit. The converted (c) C_Q and (d) σ in gravimetric units.

increase of C_Q in the positive bias range.

For practical reasons, the gravimetric C_Q and the gravimetric σ should be calculated as well. In order to convert them into a gravimetric unit, the specific surface area (*SSA*) of the pristine systems was calculated as follows:

$$SSA = \frac{SA}{\sum_i n(i)\cdot A_{r,std}(i)\cdot Da} \tag{3}$$

where *SA* is the surface area of the supercell structure, *i* represents the elements in the system, $n(i)$ the number of atoms of element *i* in the supercell structure, $A_{r,std}(i)$ the standard atomic weight of element *i*, and $Da \approx 1.661 \times 10^{-27}$ kg is the atomic mass unit.

The results are summarized in Table 2. Interestingly, silicene has the highest *SSA*. From silicene to plumbene, the *SSA* decreases because the atomic mass increases more rapidly than the atomic number. The reason for the slightly higher *SSA* of silicene than that of graphene is the ratio of the unit cell area over the atomic mass. The bond length of Si–Si in silicene is longer than that of C–C in graphene, which makes the unit cell area of silicene about 2.54 times bigger than that of graphene. However, the atomic mass of Si (28.085 atomic mass unit) is only about 2.34 times bigger than that of C (12.011 atomic mass unit). On the other hand, from silicene to plumbene, the unit cell area increases at most 1.35 times, whereas the atomic mass of each atom increases at least 1.63 times. Therefore, the *SSA* decreases from silicene to plumbene as the atomic number increases.

Table 2
Specific surface area (*SSA*) of the pristine and Ti-doped systems.

	SSA (m^2/g)	
	Pristine	Ti-doped
Ti-Graphene	2649	2448
Ti-Silicene	2778	2712
Ti-Germanene	1183	1188
Ti-Stanene	959	963
Ti-Plumbene	611	609

Fig. 3c and 3d shows the converted C_Q and σ in the gravimetric unit. As shown in Fig. 3c, the C_Q of silicene is much larger, by more than twice in the negative bias range than the C_Q of the other materials owing to its high *SSA* (compared to germanene–plumbene) and high specific C_Q (compared to graphene). From germanene to plumbene, it can be observed that the gravimetric C_Q decreased greatly, which became comparable to the gravimetric C_Q of graphene. Likewise, the gravimetric $|\sigma|$ of silicene is larger than that of other systems, more than twice in the negative bias range, as presented in Fig. 3d. However, the σ of all the pristine systems in the low bias range is still negligible. This implies that the charge accumulation is not sufficient. Therefore, pristine ETDM systems are not suitable materials for EDLCs.

3.3. Geometric and electronic properties of Ti-doped systems

In order to enhance the capacity of low voltage ETDMs, implementing new states near the E_F is required. Among the 3d transition metal atoms [37], the dopants Cu, Sc, V, Cr, and Fe severely modify the band structures, and the doped silicenes become conductive because some bands cross the E_F. The dopants Co, Ni, and Zn introduces bands, but these bands are not nearly flat bands. These bands are spread in a wide range of energy levels, thus are unable to introduce high DOS peaks required for the enhancement of quantum capacitance. The dopant Mn successfully introduces nearly flat band, but this band is placed about 0.5 eV above the E_F. In addition, another band introduced by this dopant crosses the E_F, thus making the doped silicene conductive. Only the dopant Ti introduces nearly flat bands near the E_F. At the same time, there are no bands crossing the E_F. Therefore, the dopant Ti is the most suitable dopant for the purpose of this study, so Ti doping is introduced.

The stability of the doping is estimated by calculating the formation energy (ΔE_f) using the following equation:

$$\Delta E_f = E_{Ti-ETDM} - E_{ETDM+v} - \mu_{Ti} \tag{4}$$

where $E_{Ti-ETDM}$ and E_{ETDM+v} are the calculated total energies of the Ti-doped ETDM systems without vacancy and pristine ETDM systems with

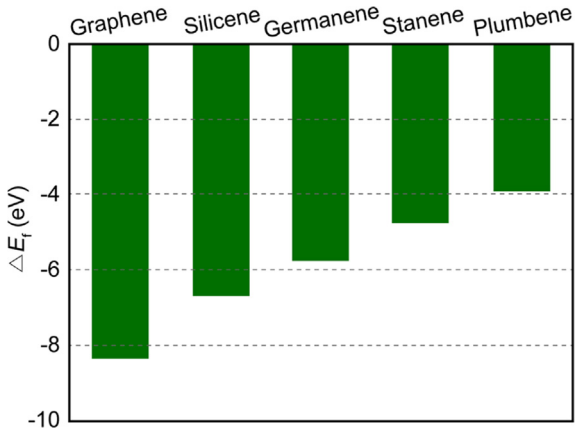

Fig. 4. Calculated formation energies (ΔE_f) of Ti-doped systems.

vacancy, respectively. The value of μ_{Ti} is the chemical potential of an isolated Ti atom. The formation energy above implies the tendency for Ti atom to be doped at the vacant site of ETDM. The formation energy of Ti-doped silicene and Ti-doped plumbene agree well with the previous results [37,44], and the dynamic stability of Ti-doped plumbene is also confirmed by the ab-initio molecular dynamics [44]. This process is experimentally feasible by first creating vacancies using focused electron beam irradiation with aberration-corrected transmission electron microscopy (AC-TEM) [45,46] or by using high energy atom bombardment [47,48] followed by doping of the Ti atom using either a solution method [45,46] or a sputtering method [47]. As shown in Fig. 4, doping the Ti atom into pristine ETDM systems is a favorable process. The final structures of Ti-doped ETDMs are shown in Fig. 5, and detailed parameters are given in Table 3. Because of the atomic size difference, protrusion and additional buckling are introduced.

To understand the effect of Ti doping on the electronic structure, we

Table 3
Geometric parameters of Ti-doped systems. X represents an atom in the group-14 elements (C, Si, Ge, Sn, or Pb) of each system. The lattice parameter of supercell is a, the bond length between the Ti atom and X atom is d_{Ti-X}, the buckling height is h_X, and the protrusion distance of the Ti atom is h_{Ti}, as indicated in Fig. 2. In Ti-doped systems, h_X is calculated as the largest z-coordinate difference between any two X atoms in each system, and h_{Ti} is calculated as the smallest z-coordinate difference between the Ti atom and an X atom.

	a (Å)	d_{Ti-X} (Å)	h_X (Å)	h_{Ti} (Å)
Ti-Graphene	9.931	1.940	0.390	1.180
Ti-Silicene	15.452	2.441	0.475	1.005
Ti-Germanene	16.181	2.500	0.736	0.769
Ti-Stanene	18.551	2.712	0.916	0.755
Ti-Plumbene	19.435	2.766	1.031	0.871

calculated the weighted electronic band structures, as shown in Fig. 6. In the weighted band structure, the weights are indicated in a color scheme from green to red, as shown in Fig. 6c. Green and red indicate the 0% and 100% contribution of the Ti atom, respectively. In order to verify the influence of the Ti atom on DOS, the projected density of states (PDOS) was also calculated and is shown together with weighted band structures in Fig. 6. We found that Ti-doping introduces a couple of flat bands near the E_F. These flat bands are mostly located on the conduction band side of the Dirac cone and introduce additional DOS. From graphene to germanene, the additional DOS is introduced as a DOS peak, whereas from stanene to plumbene, the overall DOS near the E_F is increased. This increase in DOS is mostly due to the Ti 3d orbitals, which have more states than the p orbitals of the group-14 elements. When a flat band is formed, the Dirac cone is damaged, especially on the conduction band side. The protrusion of the doped Ti atom obstructs the delocalized π bond, leading to deformation of the π bond, which plays a key role in consisting of the Dirac cone, therefore eventually opening the Dirac cone in the band structure.

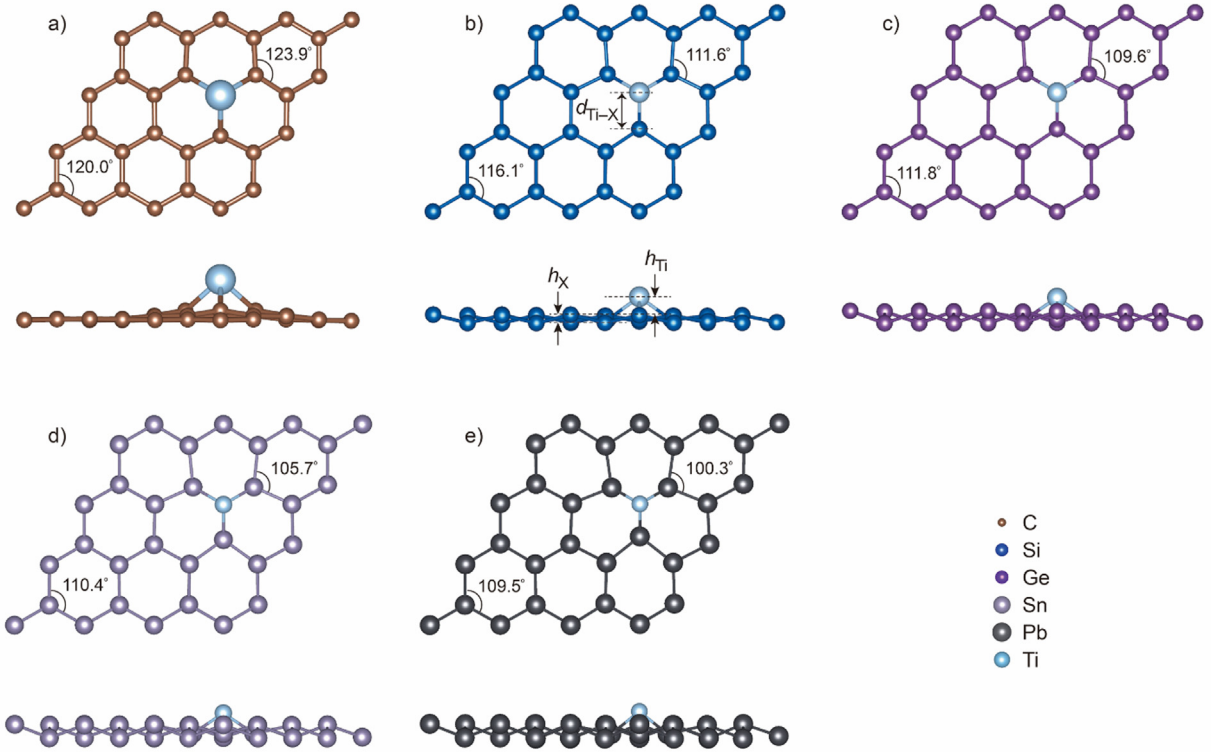

Fig. 5. Geometric structures of Ti-doped systems with a top view (top panel) and front view (bottom panel). The bond length between the Ti atom and X atom d_{Ti-X}, the buckling height h_X, and the protrusion distance of the Ti atom h_{Ti} is indicated on the structure of Ti-doped silicene, where X represents an atom in group-14 elements. Angles of the nearest and the farthest host atoms from Ti atom are also specified.

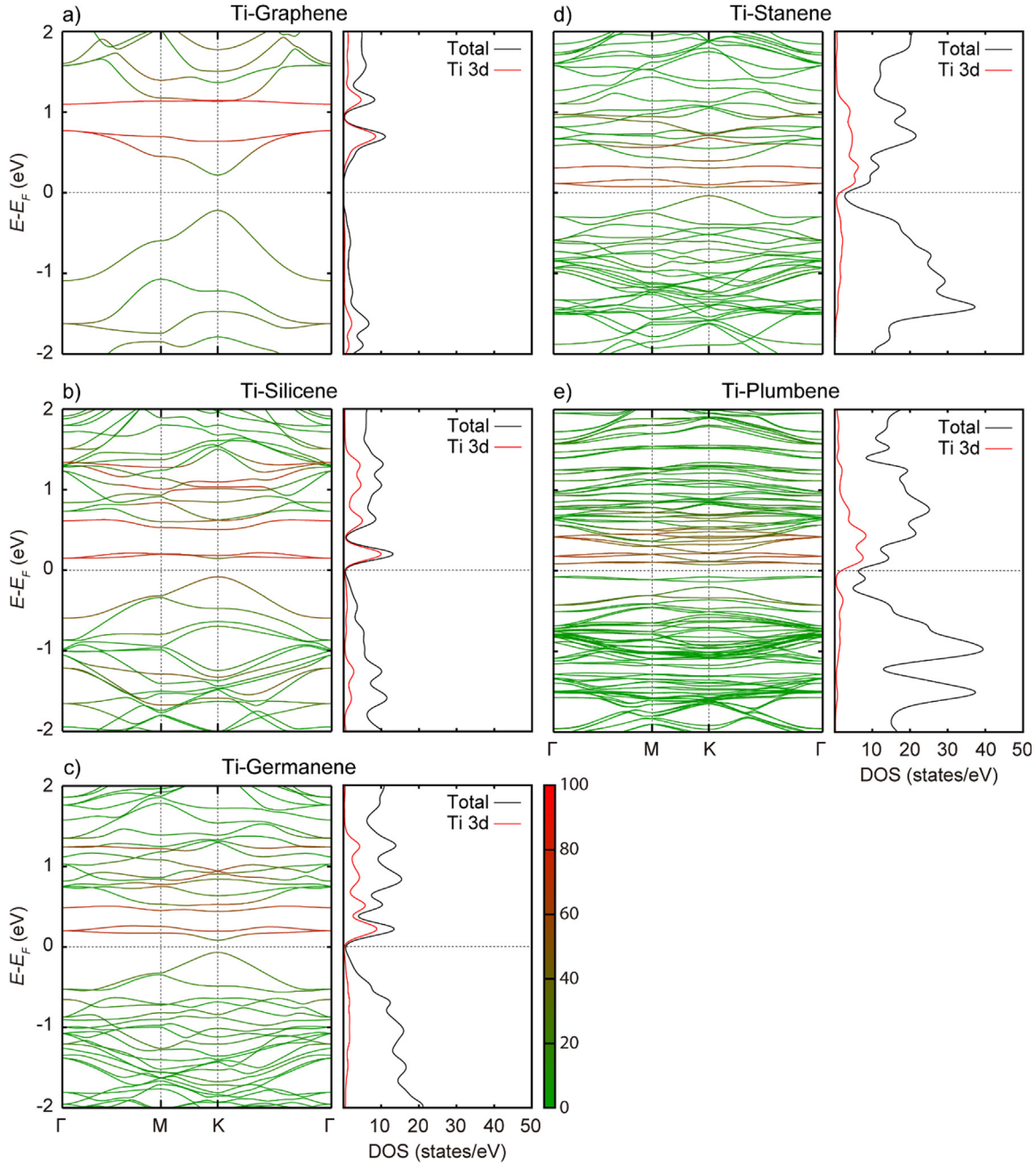

Fig. 6. Weighted electronic band structures and projected density of states (PDOS) of Ti-doped systems. The horizontal dashed lines represent the Fermi level (E_F). The color scale bar indicates the contribution of the Ti atom (%) to the band structure of each system.

3.4. Quantum capacitances and surface charges of Ti-doped systems

Fig. 7 shows the C_Q of Ti-doped ETDMs. Due to the additional DOS of Ti-doped systems near the E_F, the C_Q and the σ are enhanced overall. In Ti-doped systems from silicene to germanene, there are local maximums of C_Q around the applied bias of -0.2 V due to the Ti 3d DOS peak placed just above the E_F. However, graphene is little affected by Ti doping in the low bias range. This is because the Ti-doping level is higher than that of the systems from silicene to germanene. Instead, the local maximum of C_Q is around an applied bias of -0.7 V due to the peak of the PDOS placed at the high energy range. In the systems from stanene to plumbene, the overall increase of C_Q in the negative bias range can be observed since the DOS increased smoothly without forming any peaks. In the positive bias range, the C_Q of all the Ti-doped systems from graphene to plumbene shows a steep increase overall. Due to the DOS getting denser from the Ti-doped graphene to silicene in the range $E - E_F < 0$, the values of C_Q also increase. In Fig. 7b, the σ of Ti-doped graphene is nearly absent in the range from -0.4 to 0.4 V due to the low C_Q values of Ti-doped graphene around 0 V. On the other hand, the curves of the Ti-doped systems from silicene to plumbene have a positive slope at 0 V and show several concave-upward shapes in the negative applied potential range. Although Ti-doped graphene also has very high C_Q values around -0.7 V, the σ value hardly reaches the level of the other materials due to C_Q values in $\phi < -0.8$ V region, which dropped to too low values. This makes the $|\sigma|$ values smaller than those of the other materials from the -0.8 to -1 V range. In the positive applied potential range, σ increases steeper in the systems where the atomic number of group-14 elements is larger, except for plumbene. This can be explained by their C_Q values becoming higher from Ti-doped graphene to stanene. The σ of graphene in the positive bias range

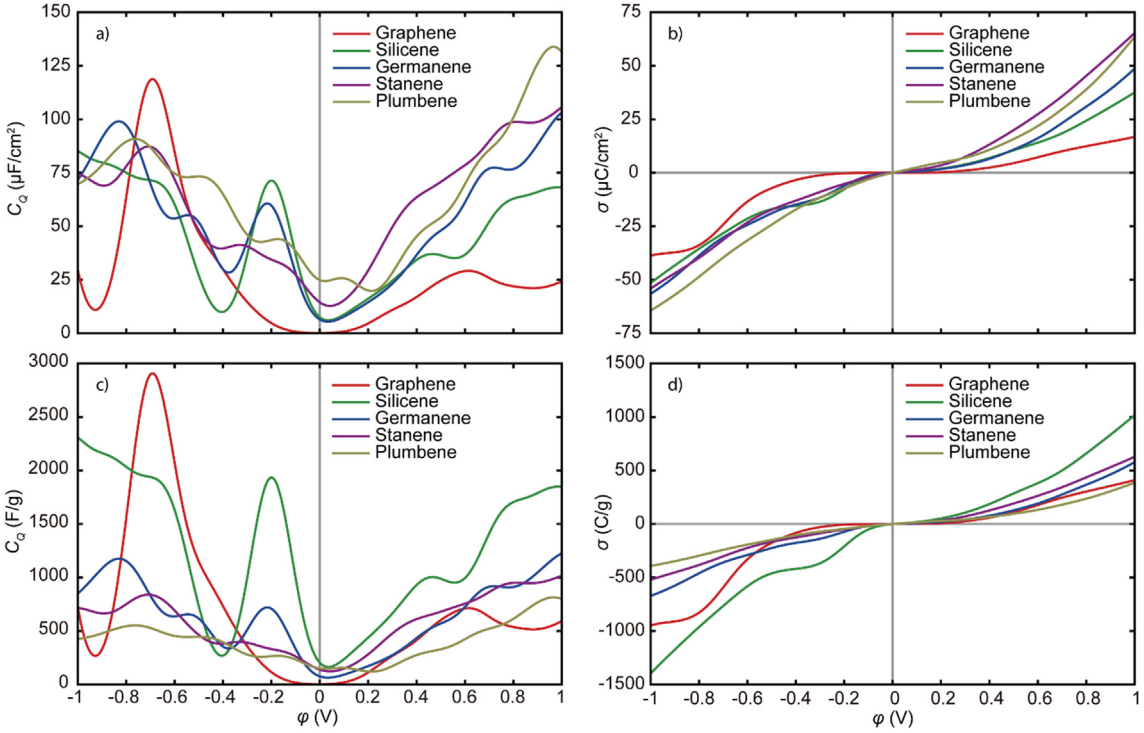

Fig. 7. (a, c) The calculated quantum capacitances (C_Q) and (b, d) the excess charge densities (σ) of Ti-doped systems with specific and gravimetric units, respectively.

just mildly increases after Ti doping without any other dominant changes.

The *SSA* of Ti-doped systems is also calculated prior to the calculations of gravimetric C_Q and σ. Table 2 shows that the *SSA* of graphene and silicene are reduced by Ti doping whereas that of other ETDMs except for plumbene slightly increases after doping. This mostly results from the contribution of the atomic weight of the Ti atom. This weight is heavier than that of the C and Si atom, which increases the weight of graphene and silicene after doping. The case of Ge, Sn, and Pb is the opposite, where the atomic weight of the Ti atom is lighter than that of the Ge, Sn, and Pb atom, which decreases the weight of germanene, stanene, and plumbene. Also, all the ETDM structures consist of 32 group-14 element atoms, but these systems are doped with just one Ti atom so that the doped Ti atoms only slightly affect the weight. In addition, the lattice parameter of the doped systems except for graphene slightly decreased due to the Ti-dopant-induced compressive strain. It was revealed that the strain increases as the atomic number increases. Therefore, the surface area of systems from silicene to plumbene decreases. The two contributions are combined, and resulted in the less increase of *SSA* of stanene than germanene, and even slightly decreased *SSA* of plumbene. Nevertheless, the overall tendency of the *SSA* of the Ti-doped systems is almost the same as the tendency of pristine systems. In other words, Ti-doped silicene has the highest *SSA* among the other Ti-doped systems.

Lastly, the gravimetric C_Q and the gravimetric σ are calculated for Ti-doped systems to determine their practicality. As can be seen from Fig. 7a and c, the ratio of C_Q of graphene and silicene is similar in the specific and in the gravimetric scale due to almost the same *SSA* of these two systems. From germanene to plumbene, the gravimetric C_Q becomes less than 1250 F/g due to the small *SSA* of these systems. Despite the high *SSA*, the graphene has even lower C_Q values than the other Ti-doped systems in the low bias range due to the scarce DOS values near the E_F. Therefore, graphene possesses the lowest gravimetric σ among the Ti-doped systems in the low bias range, as represented in Fig. 7d. This is not very practical. On the other hand, silicene shows more practical enhancement for C_Q. In particular, the gravimetric σ of silicene in the bias range presented in the figure shows the best performance among the other Ti-doped systems due to its advantage in *SSA*.

4. Conclusion

In this work, the effects of Ti-doping on the electronic structure and C_Q of 2D materials of group-14 elements are investigated. Pristine systems without any doping show the typical features of the Dirac cone, which is the reason for the lack of DOS near the E_F. In case of pristine plumbene, the SOC splits the Dirac cone and opens the band gap, which results in the absence of DOS near the E_F. This lack of DOS leads to low capacitance and low σ in the low bias range. Doping the Ti atom into the systems deforms the delocalized π bonds, resulting in the Dirac cone opening. At the same time, the 3d orbitals of the doped Ti atom introduce additional bands, mostly nearly flat bands, right above the E_F. These newly formed bands accommodate enough DOS for electrons to be stored. Consequently, high C_Q and high σ can be achieved in a low bias range by a Ti doping strategy. In addition, the highest *SSA* of Ti-doped silicene provides excellent gravimetric C_Q and gravimetric σ compared to other systems. Our results show that Ti-doping is a very effective approach to enhance C_Q of 2D materials for improving the performance of EDLCs.

CRediT authorship contribution statement

Juven Rihm: . **:** Software, Writing - original draft. **Eun Seob Sim:** Formal analysis, Writing - review & editing. **Sung Beom Cho:** Conceptualization, Supervision. **Yong-Chae Chung:** Funding acquisition, Project administration.

Declaration of Competing Interest

The authors declare that they have no known competing financial interests or personal relationships that could have appeared to influence the work reported in this paper.

Acknowledgement

This work was supported by the National Research Foundation of Korea (NRF) grant funded by the Korea government (Ministry of Science and ICT) (2019R1A2B5B01070215 and 2019R1F1A1058554). The computational resources are partially supported by Korea Supercomputing Center (KSC-2019-CRE-0023).

References

[1] D.P. Dubal, O. Ayyad, V. Ruiz, P. Gómez-Romero, Hybrid energy storage: the merging of battery and supercapacitor chemistries, Chem. Soc. Rev. 44 (7) (2015) 1777–1790.
[2] F. Su, L. Huo, Q. Kong, L. Xie, C. Chen, Theoretical study on the quantum capacitance origin of graphene cathodes in lithium ion capacitors, Catalysts 8 (10) (2018) 444.
[3] G.M. Yang, Q. Xu, X. Fan, W.T. Zheng, Quantum capacitance of silicene-based electrodes from first-principles calculations, J. Phys. Chem. C 122 (4) (2018) 1903–1912.
[4] H. Zhang, H. Guo, A. Li, X. Chang, S. Liu, D. Liu, Y. Wang, F. Zhang, H. Yuan, High specific surface area porous graphene grids carbon as anode materials for sodium ion batteries, J. Energy Chem. 31 (2019) 159–166.
[5] C. Portet, G. Yushin, Y. Gogotsi, Effect of carbon particle size on electrochemical performance of EDLC, J. Electrochem. Soc. 155 (7) (2008) A531–A536.
[6] M.D. Stoller, S. Park, Y. Zhu, J. An, R.S. Ruoff, Graphene-based ultracapacitors, Nano Lett. 8 (10) (2008) 3498–3502.
[7] B.G. Choi, M. Yang, W.H. Hong, J.W. Choi, Y.S. Huh, 3D macroporous graphene frameworks for supercapacitors with high energy and power densities, ACS Nano 6 (5) (2012) 4020–4028.
[8] Z. Liu, P.B. Balbuena, P.P. Mukherjee, Evaluating silicene as a potential cathode host to immobilize polysulfides in lithium–sulfur batteries, J. Coord. Chem. 69 (2016) 2090–2105.
[9] S.M. Seyed-Talebi, I. Kazeminezhad, J. Beheshtian, Theoretical prediction of silicene as a new candidate for the anode of lithium-ion batteries, Phys. Chem. Chem. Phys. 17 (44) (2015) 29689–29696.
[10] F.A. Chyada, A.R. Jabur, H.A. Alwan, Effect addition of graphene on electrical conductivity and tensile strength for Recycled electric power transmission wires, Energy Procedia 119 (2017) 121–130.
[11] K.I. Bolotin, K.J. Sikes, Z. Jiang, M. Klima, G. Fudenberg, J. Hone, P. Kim, H.L. Stormer, Ultrahigh electron mobility in suspended graphene, Solid State Commun. 146 (9) (2008) 351–355.
[12] Z.-G. Shao, X.-S. Ye, L. Yang, C.-L. Wang, First-principles calculation of intrinsic carrier mobility of silicene, J. Appl. Phys. 114 (9) (2013) 093712.
[13] L. Li, A. Manthiram, Dual-electrolyte lithium–air batteries: influence of catalyst, temperature, and solid-electrolyte conductivity on the efficiency and power density, J. Mater. Chem. A 1 (16) (2013) 5121–5127.
[14] G. Kresse, J. Hafner, *Ab initio* molecular dynamics for liquid metals, Phys. Rev. B 47 (1) (1993) 558–561.
[15] G. Kresse, J. Hafner, *Ab initio* molecular-dynamics simulation of the liquid-metal—amorphous-semiconductor transition in germanium, Phys. Rev. B 49 (20) (1994) 14251–14269.
[16] G. Kresse, J. Furthmüller, Efficiency of ab-initio total energy calculations for metals and semiconductors using a plane-wave basis set Comput, Mater. Sci. 6 (1) (1996) 15–50.
[17] G. Kresse, J. Furthmüller, Efficient iterative schemes for *ab initio* total-energy calculations using a plane-wave basis set, Phys. Rev. B 54 (16) (1996) 11169–11186.
[18] P.E. Blöchl, Projector augmented-wave method, Phys. Rev. B 50 (24) (1994) 17953–17979.
[19] G. Kresse, D. Joubert, From ultrasoft pseudopotentials to the projector augmented-wave method, Phys. Rev. B 59 (3) (1999) 1758–1775.
[20] J.P. Perdew, Y. Wang, Accurate and simple analytic representation of the electron-gas correlation energy, Phys. Rev. B 45 (23) (1992) 13244–13249.
[21] J.P. Perdew, J.A. Chevary, S.H. Vosko, K.A. Jackson, M.R. Pederson, D.J. Singh, C. Fiolhais, Atoms, molecules, solids, and surfaces: Applications of the generalized gradient approximation for exchange and correlation, Phys. Rev. B 46 (11) (1992) 6671–6687.
[22] J.P. Perdew, K. Burke, M. Ernzerhof, Generalized gradient approximation made simple, Phys. Rev. Lett. 77 (18) (1996) 3865–3868.
[23] S. Steiner, S. Khmelevskyi, M. Marsmann, G. Kresse, Calculation of the magnetic anisotropy with projected-augmented-wave methodology and the case study of disordered $Fe_{(1-x)}Co_x$ alloys, Phys. Rev. B 93 (22) (2016) 224425.
[24] H.J. Monkhorst, J.D. Pack, Special points for Brillonin-zone integrations, Phys. Rev. B 13 (12) (1976) 5188–5192.
[25] C. Zhan, C. Lian, Y. Zhang, M.W. Thompson, Y. Xie, J. Wu, P.R.C. Kent, P.T. Cummings, D.-E. Jiang, D.J. Wesolowski, Computational insights into materials and interfaces for capacitive energy storage, Adv. Sci. 4 (7) (2017) 1700059.
[26] M. Krawiec, Functionalization of group-14 two-dimensional materials, J. Phys. Condens. Matter 30 (23) (2018) 233003.
[27] Z.-Q. Huang, C.-H. Hsu, F.-C. Chuang, Y.-T. Liu, H. Lin, W.-S. Su, V. Ozolins, A. Bansil, Strain driven topological phase transitions in atomically thin films of group IV and V elements in the honeycomb structures, New J. Phys. 16 (10) (2014) 105018.
[28] W.-F. Tsai, C.-Y. Huang, T.-R. Chang, H. Lin, H.-T. Jeng, A. Bansil, Gated silicene as a tunable source of nearly 100% spin-polarized electrons, Nat. Commun. 4 (1) (2013) 1500.
[29] L. Matthes, O. Pulci, F. Bechstedt, Massive Dirac quasiparticles in the optical absorbance of graphene, silicene, germanene, and tinene, J. Phys. Condens. Matter 25 (39) (2013) 395305.
[30] H. Şahin, S. Cahangirov, M. Topsakal, E. Bekaroglu, E. Akturk, R.T. Senger, S. Ciraci, Monolayer honeycomb structures of group-IV elements and III-V binary compounds: First-principles calculations, Phys. Rev. B 80 (15) (2009) 155453.
[31] H. Sahin, F.M. Peeters, Adsorption of alkali, alkaline-earth, and 3*d* transition metal atoms on silicene, Phys. Rev. B 87 (8) (2013) 085423.
[32] S. Cahangirov, M. Topsakal, E. Aktürk, H. Şahin, S. Ciraci, Two- and One-Dimensional Honeycomb Structures of Silicon and Germanium, Phys. Rev. Lett. 102 (23) (2009) 236804.
[33] L. Pan, H.J. Liu, Y.W. Wen, X.J. Tan, H.Y. Lv, J. Shi, X.F. Tang, First-principles study of monolayer and bilayer honeycomb structures of group-IV elements and their binary compounds, Phys. Lett. A 375 (3) (2011) 614–619.
[34] Y. Wang, Y. Ding, Strain-induced self-doping in silicene and germanene from first-principles, Solid State Commun. 155 (2013) 6–11.
[35] R. Quhe, R. Fei, Q. Liu, J. Zheng, H. Li, C. Xu, Z. Ni, Y. Wang, D. Yu, Z. Gao, J. Lu, Tunable and sizable band gap in silicene by surface adsorption, Sci. Rep. 2 (2012) 853.
[36] Z. Ni, H. Zhong, X. Jiang, R. Quhe, G. Luo, Y. Wang, M. Ye, J. Yang, J. Shi, J. Lu, Tunable band gap and doping type in silicene by surface adsorption: towards tunneling transistors, Nanoscale 6 (13) (2014) 7609–7618.
[37] Y. Lee, K.-H. Yun, S.B. Cho, Y.-C. Chung, Electronic properties of transition-metal-decorated silicene, ChemPhysChem 15 (18) (2014) 4095–4099.
[38] J. Sivek, H. Sahin, B. Partoens, F.M. Peeters, Adsorption and absorption of boron, nitrogen, aluminum, and phosphorus on silicene: Stability and electronic and phonon properties, Phys. Rev. B 87 (8) (2013) 085444.
[39] C.-C. Liu, H. Jiang, Y. Yao, Low-energy effective Hamiltonian involving spin-orbit coupling in silicene and two-dimensional germanium and tin, Phys. Rev. B 84 (19) (2011) 195430.
[40] E. Cinquanta, E. Scalise, D. Chiappe, C. Grazianetti, B. van den Broek, M. Houssa, M. Fanciulli, A. Molle, Getting through the Nature of Silicene: An sp2–sp3 Two-Dimensional Silicon Nanosheet, J. Phys. Chem. C 117 (32) (2013) 16719–16724.
[41] D. Jose, A. Datta, Understanding of the Buckling Distortions in Silicene, J. Phys. Chem. C 116 (46) (2012) 24639–24648.
[42] R. John, B. Merlin, Theoretical investigation of structural, electronic, and mechanical properties of two dimensional C, Si, Ge, Sn, Crystal Structure Theory and Applications 5 (3) (2016) 43–55.
[43] C. Kamal, A. Chakrabarti, A. Banerjee, Ab initio investigation on hybrid graphite-like structure made up of silicene and boron nitride, Phys. Lett. A 378 (16) (2014) 1162–1169.
[44] D. Hashemi, H. Iizuka, Magnetic properties of 3d transition metal (Sc–Ni) doped plumbene, RSC Adv. 10 (12) (2020) 6884–6892.
[45] A.W. Robertson, B. Montanari, K. He, J. Kim, C.S. Allen, Y.A. Wu, J. Olivier, J. Neethling, N. Harrison, A.I. Kirkland, J.H. Warner, Dynamics of single Fe atoms in graphene vacancies, Nano Lett. 13 (4) (2013) 1468–1475.
[46] Z. He, K. He, A.W. Robertson, A.I. Kirkland, D. Kim, J. Ihm, E. Yoon, G.-D. Lee, J.H. Warner, Atomic structure and dynamics of metal dopant pairs in graphene, Nano Lett. 14 (7) (2014) 3766–3772.
[47] H. Wang, Q. Wang, Y. Cheng, K. Li, Y. Yao, Q. Zhang, C. Dong, P. Wang, U. Schwingenschlögl, W. Yang, X.X. Zhang, Doping monolayer graphene with single atom substitutions, Nano Lett. 12 (1) (2012) 141–144.
[48] Z. Bai, L. Zhang, L. Liu, Bombarding graphene with oxygen ions: combining effects of incident angle and ion energy to control defect generation, J. Phys. Chem. C 119 (47) (2015) 26793–26802.